

Implementation and application of a novel 2D magnetic twisting cytometry based on multi-pole electromagnet

La Chen, Vanessa Maybeck, Andreas Offenhäusser, and Hans-Joachim Krause

Citation: Review of Scientific Instruments 87, 064301 (2016); doi: 10.1063/1.4954185

View online: http://dx.doi.org/10.1063/1.4954185

View Table of Contents: http://scitation.aip.org/content/aip/journal/rsi/87/6?ver=pdfcov

Published by the AIP Publishing

Articles you may be interested in

Adhesion patterning by a novel air-lock technique enables localization and in-situ real-time imaging of reprogramming events in one-to-one electrofused hybrids Biomicrofluidics **10**, 054122 (2016); 10.1063/1.4965422

Mapping power-law rheology of living cells using multi-frequency force modulation atomic force microscopy Appl. Phys. Lett. **107**, 173702 (2015); 10.1063/1.4934874

Towards an on-chip platform for the controlled application of forces via magnetic particles: A novel device for mechanobiology

J. Appl. Phys. 117, 17B317 (2015); 10.1063/1.4917191

Benchtop fabrication of multi-scale micro-electromagnets for capturing magnetic particles

Appl. Phys. Lett. 105, 074102 (2014); 10.1063/1.4893564

A novel pneumatic micropipette aspiration method using a balance pressure model

Rev. Sci. Instrum. 84, 123703 (2013); 10.1063/1.4832979





Implementation and application of a novel 2D magnetic twisting cytometry based on multi-pole electromagnet

La Chen, Vanessa Maybeck, Andreas Offenhäusser, and Hans-Joachim Krause^{a)} *Institute of Bioelectronics (ICS-8/PGI-8), Forschungszentrum Jülich GmbH, Jülich 52425, Germany*

(Received 15 February 2016; accepted 5 June 2016; published online 21 June 2016)

We implemented a novel 2D magnetic twisting cytometry (MTC) based on a previously reported multi-pole high permeability electromagnet, in which both the strength and direction of the twisting field can be controlled. Thanks to the high performance twisting electromagnet and the heterodyning technology, the measurement frequency has been extended to the 1 kHz range. In order to obtain high remanence of the ferromagnetic beads, a separate electromagnet with feedback control was adopted for the high magnetic field polarization. Our setup constitutes the first instrument which can be operated both in MTC mode and in magnetic tweezers (MT) mode. In this work, the mechanical properties of HL-1 cardiomyocytes were characterized in MTC mode. Both anisotropy and lognormal distribution of cell stiffness were observed, which agree with our previous results measured in MT mode. The response from these living cells at different frequencies can be fitted very well by the soft glassy rheology model. *Published by AIP Publishing*. [http://dx.doi.org/10.1063/1.4954185]

I. INTRODUCTION

The log-normal distribution of cell stiffness has been frequently reported. 1-4 One of the reasons for the large variation is the inherent complexity and high heterogeneity of cell structure.⁵⁻⁷ The probe response also depends on its linkage to the cell, for example, the probe type, probe coating, and binding geometry were found to have significant effects on the cell mechanical moduli.^{8,9} Hence, it is difficult to compare the cell stiffness measured by different microrheologies directly. However, the elastic moduli-frequency curves of cell measured by different methods can be rescaled (i.e., shifted in log-scale coordinates) to compare them. ⁹ Therefore, multi-sample and multi-frequency measurements are usually favorable for cell mechanics studies. Compared to other microrheological techniques, atomic force microscopy (AFM) and optical tweezers exhibit a very high resolution. Therefore, they are widely used in single molecular and cell mechanics studies. 10 In AFM, however, only a single probe can be applied at a time. In the case of optical tweezers, it is also very hard to sample many cells at a time. In addition, the high intensity laser can cause damage to the cell organelles.¹⁰ Although passive microrheologies such as the two point microrheology inherently adopt multi-probe measurements, they are susceptible to experimental conditions. 11 Recently we implemented a high throughput electromagnetic tweezers and successfully realized multi-cell measurements. 4 However, a trade-off between high force and throughput (size of workspace) must been made. 12 Unlike the high gradient magnetic field which is essential for high force magnetic tweezers (MT), ¹³ in magnetic twisting cytometry (MTC), only a small uniform magnetic field is used to twist the prepolarized ferromagnetic beads. 14 Therefore, it is much easier to implement a multi-cell measurement in MTC. Since the appearance of this tool, it has been widely used to investigate the mechanical properties of individual adherent cells.^{6,15–17} Unlike the traditional MTC, which used a magnetic field sensor to detect the bead rotation, ^{15,16} in the optical MTC, the lateral displacement of a probe caused by rotation is detected by a camera. Thus, it combines the advantages of high throughput and single cell studies.^{6,17} Moreover, thanks to the heterodyning technology, the measurement frequency range of optical MTC has been extended to the kHz range.¹⁷

In order to generate the twisting field, MTC usually adopts Helmholtz coils, which could cause too much heat under high currents. Most MTCs implement a single group of twisting coils which can only apply the twisting field in a single direction. However, multi-dimensional actuation is especially useful for cells with a definite morphologic polarity or cytoskeletal anisotropy. Hu et al. realized a 3D MTC with three groups of Helmholtz coils. 18 With a high performance soft magnetic yoke, both the exciting current and the size of the actuator can be decreased, thus easily allowing multi-dimensional actuation.¹³ However, as far as we know, a MTC apparatus based on electromagnets has not been reported. On the other hand, single turn Helmholtz coils are widely used to directly polarize the ferromagnetic beads on-site with the help of a surge generator. 14,16 However, for small size samples, the electromagnet is a low cost solution that allows achievement of a high magnetic field easily.

In this paper, we introduce an optical MTC system based on our previously published magnetic tweezers setup. ¹³ Both polarization and twisting magnetic field are based on electromagnets. A separate electromagnet was utilized to magnetize the ferromagnetic particles bound to the surface of the cells. The existing yoke electromagnet, but without tips, was used to apply the twisting magnetic field. With this MTC

a) Author to whom correspondence should be addressed. Electronic mail: h.-j.krause@fz-juelich.de.

setup, the mechanical properties of cardiomyocyte HL-1 cells were examined under different conditions.

II. MATERIALS AND METHODS

A. Experimental setup

In this work, the MTC setup is based on the previously reported multi-pole electromagnetic tweezers. 4,12,13 The diagram of this setup is presented in Fig. 1(a). The control and data acquisition (DAQ) for twisting beads are marked with red arrows. The twisting electromagnet consists of a main hexapole yoke, a group of actuating coils, and a fluidic reservoir. The details are shown in Figs. 1(b) and 1(c). The fluidic reservoir containing cell samples is located on the top central area and enclosed by the symmetric magnetic poles. As shown in Figs. 1(b) and 1(c), the twisting magnetic field (Bt) along the y and x axis can be generated with different combinations of coil currents. The rotation of vertically magnetized beads under a twisting field along the x axis is shown in Fig. 1(d). In order to achieve good resolution, a water immersion non-magnetic objective (W Plan-Apochromat $40\times/1.0$ DIC, Carl Zeiss AG, Germany) mounted on an upright microscope (Axio Scope.A1, Carl Zeiss AG, Germany) was used. The cell samples were

illuminated with transmitted light from the bottom. The bright field images were captured using a sCMOS (Scientific Complementary Metal-oxide-semiconductor) camera (Zyla 5.5, Andor Technology Ltd., UK). In order to decrease the distortion of bead images under high speed twisting, global shutter was employed for the image exposure. The exposure time for each image was set to 0.15 ms. Pixel binning (2×2) was used to improve the signal-to-noise ratio of image. The displacements of beads were analyzed after measurement by a 2D cross correlation algorithm, 4,13 which yields an accuracy of about 10 nm. A DAQ card (USB-6259, National Instruments Corporation, USA) was used to generate sinusoidal stimuli signals, which was connected to a power amplifier to drive the twisting electromagnet. In order to achieve a high timing precision, the stimuli signals generated by the DAQ card were refreshed at 100 kHz. A heterodyning technique was adopted to detect the periodic movement of beads at high frequency.¹⁷ Both the camera and the DAQ card were controlled via a customized LabVIEW (National Instruments, USA) software implemented on a computer which was equipped with a high performance CPU (Core i7 3770K, Intel Corporation, USA) and 32 GB RAM. During experiment, the raw image data read off the camera were quickly streamed into a pre-allocated buffer. Image acquisition, image processing, and stimuli signal generation were performed in three parallel threads.

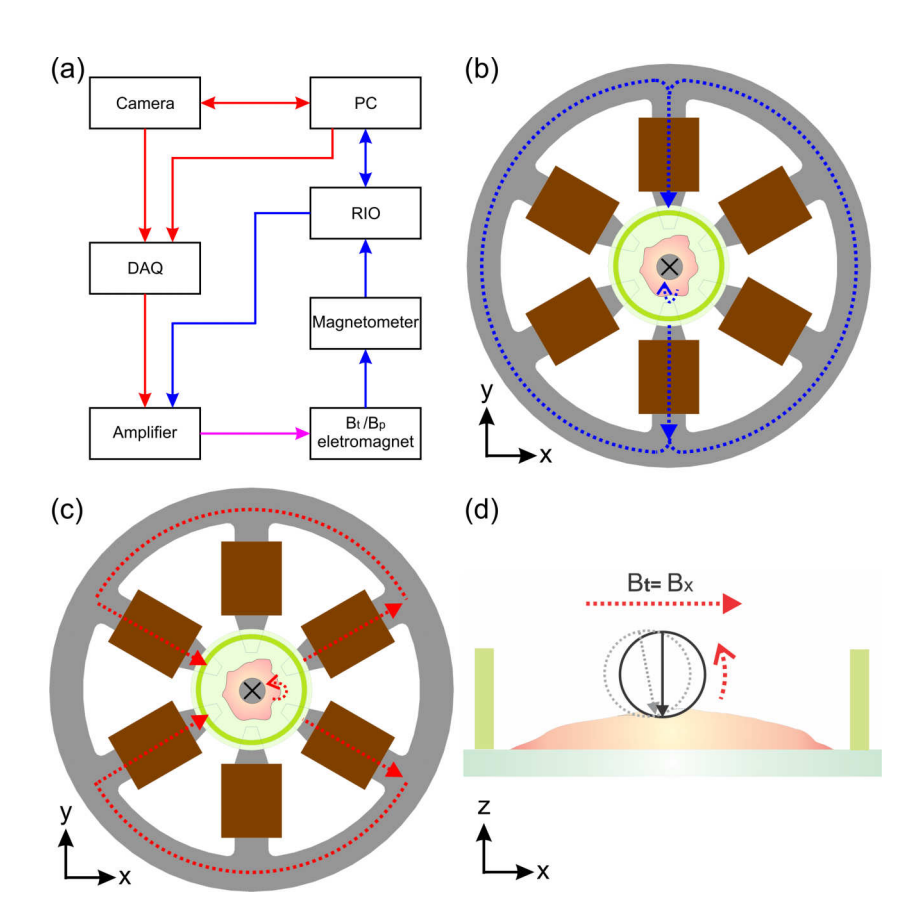


FIG. 1. (a) Block diagram of setup. The red arrows refer to the control/data flow of B_t , and the blue arrows denote the control/data flow of B_p . The B_t and B_p share the control/data flow depicted by the pink arrow. (b) Schematic of the twisting apparatus. Coils, yoke, and fluidic reservoir are depicted in brown, grey, and green, respectively. The fluidic reservoir is composed of a cover slip and a glass ring. The blue dotted lines in the yoke show the magnetic flux for a twisting field along the y axis. (c) The red dotted lines in the yoke show the magnetic flux for a twisting field along the x axis. (d) This schematic shows the rotation of a vertically polarized bead under the twisting field along the x axis. The gray dotted circle indicates the position of bead after the application of twisting field. The drawings are not to scale.

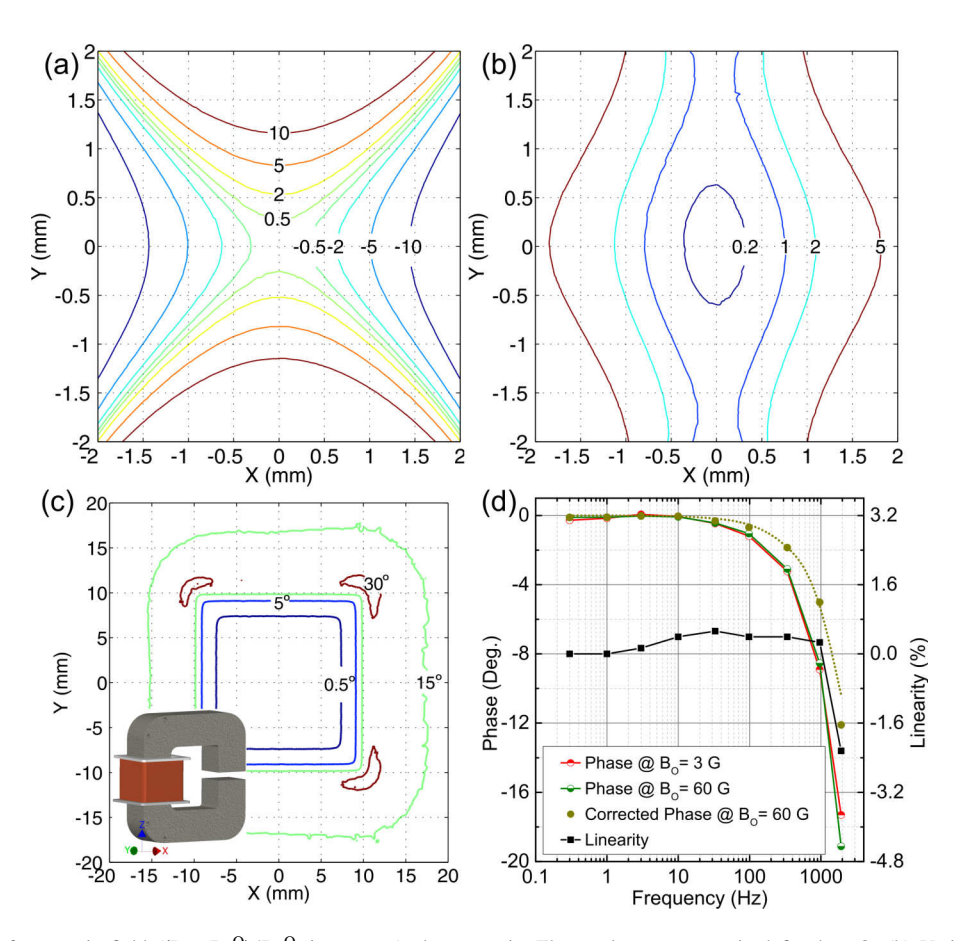


FIG. 2. (a) Variation of magnetic field $((B_v - B_v^O)/B_v^O)$, in percent) along y axis. The workspace center is defined as O. (b) Variation of magnetic field $((B_x - B_x^0)/B_x^0)$, in percent) along x axis. (c) The direction (angle off the z axis in degrees) of magnetic field in the polarization electromagnet (20×20 mm²) in cross section). The inset depicts the mechanical drawing of the polarization electromagnet. Red, silver, and gray colors depict coil, coil former, and St37 steel, respectively. (d) Phase shift and linearity of twisting magnetic field. The linearity is calculated according to the magnetic field at 1 Hz. The phase shift represented by the red and green lines includes all parts: yoke, amplifier, and magnetometer. The brown dots represent the corrected phase shift in which the contribution from the magnetometer was removed. The brown dotted line shows the fitting of the phase shift below 1 kHz to a single pole transfer function.

In practice, the cell sample can be either cultured on a cover slip and then be placed into a fluidic reservoir for measurement or it can be cultured directly on the fluidic reservoir. Before measurement, the magnetic beads were bound on the cells and magnetized in a high vertical magnetic field (B_n), which was generated with a polarization electromagnet (see inset in Fig. 2(c)). It was made of common St37 construction steel with a 5 mm gap in the yoke serving as the workspace. In one corner of the workspace, there was a small Hall sensor installed. A feedback control loop based on a multifunction RIO card (PCIe-7841R, National Instruments Corporation, USA) was implemented, which allows the device to achieve a magnetic field accuracy of 0.5 G. The items used for magnetizing the beads are marked by blue arrows in Fig. 1(a). Both the twisting and the polarization electromagnets shared the same custom multi-channel power amplifier. The details of the amplifier and magnetometer can be found in Ref. 13.

B. Magnetic tweezers mode

As mentioned in the Introduction, our setup can work in either MTC or MT mode. It is well known that the translation force generated in MT is dependent on the magnetic field

gradient. When the device works in MT mode, a specific fluidic reservoir with 3 sharp magnetic tips should be adopted. The workspace is symmetrically encompassed by the three tips which are 120° apart. These magnetic tips (0.1 mm thick) are made from material with high saturation magnetization B_s and are fixed between the cover slip and glass ring with PDMS (polydimethylsiloxane). In order to apply an accurate force on the magnetic particle, superparamagnetic beads (with nonhysteresis magnetization) are usually used in MT. The polarization electromagnet in MTC is not necessary for MT experiment. Most of the hardware is shared between the MT and MTC work modes, but the control software is different. More details of the MT can be found in our published papers. 4,12,13

C. Magnetic field generation

In MTC, it is important to generate a uniform magnetic field, not a high magnetic gradient field as in MT. With a homogeneous magnetic field, both torque error and the effect from translational force can be reduced. In this work, we examined the magnetic field distribution in the workspaces of twisting and polarizing electromagnets using finite element simulation. The details of the simulation can be found in Ref. 12. In order to decrease the leakage of magnetic flux, the 6 poles of the twisting electromagnet were paired into 3 groups of oppositely oriented poles. As shown in Fig. 1(b), for example, the pair of poles along the y axis is used to generate a magnetic field along the y axis. The corresponding magnetic field distribution is presented in Fig. 2(a). The maximum magnetic field variation within 1×1 mm² is less than 2%. With a coil current of 100 A turns, the magnetic field at the center of the simulation and in the experiment (measured by Gauss meter), is 83.0 and 80.8 G, respectively. The small difference between simulation and experimental measurement may originate from the approximation of the simulation geometry and from the practical position of the magnetic probe in the measurement which amounts to about 1 G accuracy in measurement. Due to the high permeability of the yoke and the good heat performance of the setup, 13 the measured temperature increase at the coils was less than 1 °C during experiments. Hence, the heating effect on the cells was negligible. The magnetic field along the x axis can be generated adopting 2 pairs of poles with the same coil current, as shown by the red dotted lines in Fig. 1(c). If the magnetic field is generated by two pairs of poles, it has a better uniformity than in the case of a single pair of poles, as shown in Fig. 2(b). For example, the magnetic field variation within $1 \times 1 \text{ mm}^2$ is less than 0.7% when using two pairs of poles. In addition, the magnetic field changes more slowly along the y axis. Thanks to the large gap (10 mm) between the yoke poles, the planar twisting magnetic field also changes slowly along the z axis (vertical direction). For instance, the magnetic field B_v (O refers to the workspace center) only decreases about 2.7% at a distance of 0.5 mm above the fluidic reservoir. On the other hand, the torque applied on the beads also depends on the magnetic moment of the beads (see the Eq. (2)). In order to obtain the maximum magnetic moment, the polarization magnetic field should be strong enough to magnetize the ferromagnetic beads along its main M-H loop. In this situation, the final magnetic moment of the beads does not depend on the strength of the polarization field any more. It is very important to magnetize all the beads in the same direction. As presented in Fig. 2(c), it is obvious that the magnetic field in our polarization electromagnet exhibits a very well defined direction in the central workspace. The directional variation of the magnetization field is less than 1° in a 15×15 mm² area. The non-vertical field components increase when approaching the corner or the edge of the yoke. The ratio of magnetic field to coil current in the workspace is about 1000 G/400 A turns. Besides this, there is a non-negligible remnant magnetic field after the coil current is turned off because of the hysteresis of the steel core. In order to reduce this effect, the feedback

control is activated to set the magnetic field to zero after bead magnetization.

In addition to the static features, the dynamic properties of the twisting field also have significant influence on the measurement result. Because of the loss modulus feature of the cells, the response from the cells usually has some phase lag. Any phase error caused by the setup should be canceled out. For the twisting magnet, the phase shift and linearity of the magnetic field at different frequencies were measured with another DAQ card (the same type as the one used for the generation of the B_t signal), which acquired the B_t signal and the magnetic field signal measured by the magnetometer synchronously. The results are shown in Fig. 2(d). Thanks to the multi-layer structure of the yoke, 13 the phase lag at low frequencies (<100 Hz) was very small. The linearity was also very good at all frequencies below 1 kHz. For frequencies below 1 kHz and magnetic fields below 100 G, the phase lag and the linearity were almost independent of the strength of the magnetic field. With higher frequency, the phase shift increased quickly and deviated from the single pole model $(f_c = 10.5 \text{ kHz})$ behavior. This large phase lag was caused by the eddy current effect, which increases quickly at high frequencies. 19

D. Heterodyning

According to the Nyquist sampling theorem, the bead movement can be only detected when the camera acquisition frequency is at least equal or larger than 2 times the frequency of bead movement or twisting magnetic field. However, when the bead movement is sinusoidal, it can be detected by choosing a special camera acquisition frequency and twisting magnetic field frequency even if the twisting frequency is higher than the camera frequency. The amplitude and the phase lag of bead movement can be deduced by fitting to the formula $d \times \sin(\omega t + \varphi)$, like in the low frequency case. This method is called heterodyning technique. When using this technique, the operation of different devices should be synchronized very accurately. The frequency resolution and stability of both stimuli and detection are very important for the precision of results. Although the maximal jitter of our camera is about 1 μ s, which is larger than the DAQ card's (~50 ns), it is accurate enough for the detection of beads' movement with frequency ≤ 1 kHz.

The pre-set measurement parameters used in this work are listed in Table I. The camera acquisition frequency f_A was set according to the twisting frequency f_T as

$$f_T - Nf_A = 1/T_M. (1)$$

TABLE I. Heterodyning technique: frequency, cycle, and period.

Twisting frequency (Hz)	0.03	0.1	0.3	1	3	10	33	98	338	962
Camera acquisition frequency (Hz)	0.96	3.2	9.6	32	48	9.6	32	48	48	48
Measurement cycles	3	3	3	3	5	5	5	10	20	20
Measurement period (s)	100/3	10	10/3	1	1/3	2.5	1	0.5	0.5	0.5
Number of images	96	96	96	96	90	120	160	320	480	480

Here, N denotes an integer multiple and T_M is the measurement period. Only when f_T was larger than 3 Hz, the heterodyning was adopted. The camera was set to work at the highest speed to make the measurement time as short as possible. As listed in Table I, the number of images at each frequency is deduced from $f_A \times T_M \times$ cycle. In the measurement of each frequency, the waveform generation of twisting field by DAQ was triggered to start by the camera's exposure signal of the first image.

E. Mechanical model

In MTC, the magnetic bead is bound to the cells' intracellular cytoskeleton via the cell receptors of extracellular matrix such as integrins. Hence, the response of bead reflects the mechanical properties of the cell. The specific torque on the bead can be defined as the mechanical torque per unit bead volume.²⁰ For convenience, it can be written as

$$T = cB_t \cos \theta. \tag{2}$$

Here, c is a factor depending on the bead's magnetic moment and size; θ refers to the angle between the bead's magnetic moment and the twisting field B_t . The ferromagnetic beads (CFM-40-10, Spherotech, Inc., USA) used in this work have a mean diameter of 4.47 μ m. When the polarization field B_p is as high as 2000 G, a maximum residual magnetic moment of 4.3×10^{-13} Am²/bead can been obtained.²¹ With these data, we can deduce the parameter c = 0.93 Pa/G.

In order to obtain the traditional elastic shear (G') and loss (G'') moduli, a geometric factor α is usually adopted, ²⁰ by which the complex elastic modulus can be deduced from the bead displacement ($\tilde{G} = \alpha T/\tilde{d}$). In systematic studies, Fabry *et al.* found that the mechanics of living cell cytoskeleton follow the soft glassy rheology model (SGR). ^{6,17} The complex elastic modulus of a cell obeys ¹⁷

$$\tilde{G}(\omega) = G_0 \left(\frac{\omega}{\Phi_0}\right)^{x-1} (1+i\eta) \Gamma(2-x) \cos\frac{\pi}{2} (x-1) + i\omega\mu.$$
(3)

 G_0 and Φ_0 are scale factors. ω is the angular frequency of the twisting field. Parameter η is the structural damping coefficient, ¹⁷

$$\eta = \frac{\tan(x-1)\pi}{2}.\tag{4}$$

In formulas (3) and (4), x and μ are the power-law exponent and the viscosity, respectively. The power-law exponent x reflects the intracellular agitation, which is also expressed as noise temperature.

F. Cell sample preparation

1. Cell culture and bead coating

HL-1 cells were seeded on cover slips that were sterilized with flame. The mechanical experiments were carried out after 2-3 days of culture in supplemented Claycomb's medium

(10% fetal bovine serum, 0.1 mM norepinephrine, 2 mM L-glutamine, and 100 U/ml penicillin/streptomycin). The beads were coated with 50 μ g/ml fibronectin according to the procedure recommended by the manufacturer as follows: (1) add 1 ml beads, 1 ml 0.05 M MES (2-(Nmorpholino) ethanesulfonic acid, pH 5.0), 50 µg fibronectin, and 2.5 mg EDC (1-ethyl-3(-3-dimethylaminopropyl) carbodiimide hydrochloride) into a centrifuge tube, (2) vertex and incubate for 2 h at room temperature on a shaking mixer, (3) centrifuge at 3000× g for 15 min, (4) remove the supernatant carefully, (5) resuspend the pellet in 2 ml PBS (phosphate-buffered saline), (6) repeat the steps 3 and 4 and resuspend the pellet in 1 ml of PBS, and (7) keep the beads in a fridge at 4°C for use up to 1 week. Before the experiments, the supplemented Claycomb's medium was replaced by Dulbecco's Modified Eagle Medium (DMEM), in which the coated beads were mixed at a concentration of about 2×10^6 beads/ml. After 15 min incubation, the unattached beads were washed out with fresh warm DMEM twice. The change to DMEM was required to prevent passivation of the adherent coating on the beads by serum components in the supplemented Claycomb's medium.

2. Drug treatment

For drug treatment samples, the cells were first cultured and bound with beads in the same way as the control samples. Cells were then treated with either blebbistatin or paraformaldehyde. For myosin inhibition, after washing the unbound beads, fresh DMEM with $50~\mu\text{M}$ blebbistatin was added into the cell culture and incubated for additional 20 min. In order to fix the cells, they were washed twice with warm PBS, and chemically fixed with 4% paraformaldehyde in PBS for 30 min at room temperature. Then the cells were washed three times with PBS.

III. RESULTS AND DISCUSSION

A microscope image of the cells within workspace is shown in Fig. 3(a). Limited by the size of the camera sensor, the actual measurement area was $300 \times 300 \ \mu \text{m}^2$. Although there were some beads in clusters, most beads were distributed over the cells evenly and adhered to their surface. In the bead movement analysis, only the individual separated beads were considered. The bead clusters and the beads sitting near the edges of cells were ignored. Because this type of bead has a large size distribution, very big and very small beads were also not included in the analysis. Fig. 3(b) shows a scanning electron microscope (SEM) image of HL-1 cells with bound beads. The samples were prepared according to the procedure described in Ref. 4. The bead at the right of the image has a larger size than the other beads. The individual beads clearly show different embedding depths. The beads near the periphery of the cell body usually have a weak bond with their cell, as shown in the inset. As described in Ref. 22, the geometric factor α used for complex

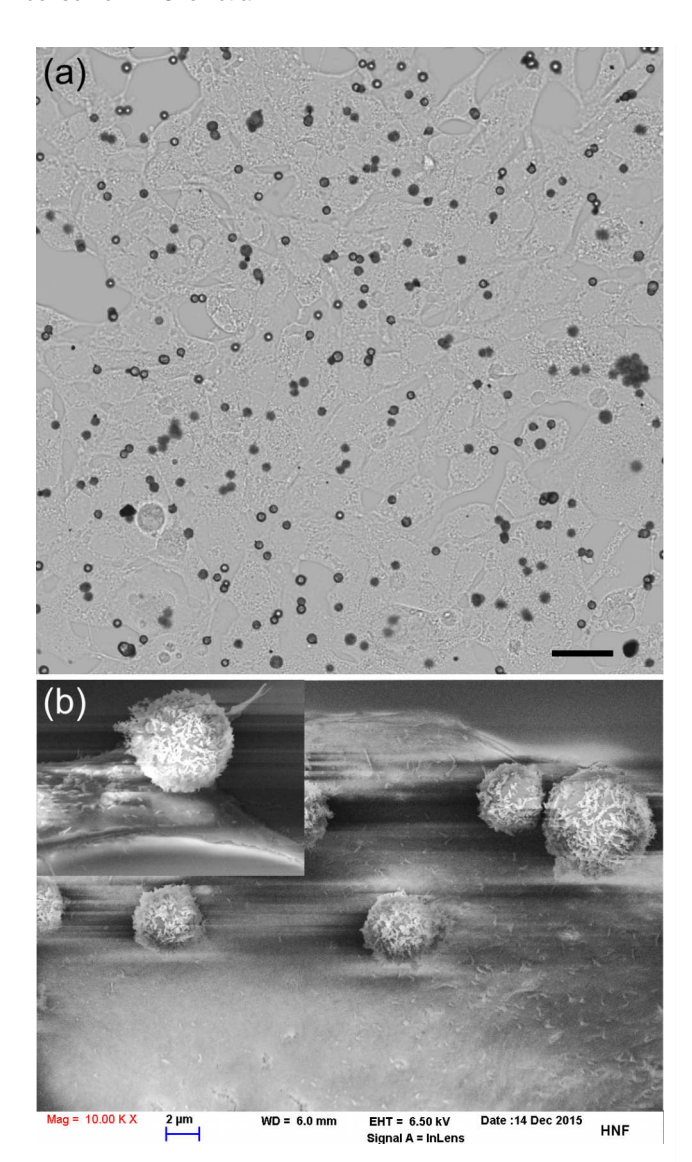


FIG. 3. (a) Microscope image of cells within workspace. Scale bar 30 μ m. (b) SEM image of beads on HL-1 cell. Inset shows a bead bound on the periphery of a cell.

elastic modulus deduction strongly depends on the local geometry of the cell and on the degree of bead embedding. For simplicity, we adopt a geometry factor of $\alpha = 6.8$ as used in Ref. 17, which is based on the assumption that 10% of the bead diameter is embedded in a 5 μ m thick cell.

Before measurement, the cell sample was first magnetized vertically using a 2000 G magnetic field produced by the polarization electromagnet. Then the sample was transferred to the twisting apparatus. A group of specific frequencies, which range from 0.03 Hz to 962 Hz as listed in Table I, were used for twisting the beads. The beads with displacement larger than 2 μ m or less than 10 nm were not included in the statistics. Displacements larger than 2 μ m indicate that the beads failed to adhere to the cells. Displacements below 10 nm are too small to achieve accurate measurements. Only the beads with a phase lag falling into the range from 0 to -90° were considered. In order to decrease the effect from magnetic relaxation, ¹⁵ the whole measurement process

was finished in less than 10 min. As presented in Fig. 4(a), the amplitude of bead displacement at different frequencies increases proportionally to the twisting magnetic field. However, when the twisting field is small (e.g., $B_t < 30$ G), the phase lag at high frequency has a large fluctuation. This may be caused by the small displacement of the beads, which is close to the detection limit. Therefore, a twisting field B_t of 30 G was used in this work unless indicated otherwise. As in Fig. 4(b), the mechanical properties of the HL-1 cell are anisotropic along different directions, in agreement with the result found with magnetic tweezers.⁴ As discussed in the Introduction, the amplitude of bead response obeys a log-normal distribution, see Fig. 4(c). In addition, both the displacement distribution and the phase lag distribution can be fit by Gaussian functions very well, as shown in Figs. 4(c) and 4(d).

As in Fig. 5, according to the formula (3), the blue solid and dashed lines denote the fitting results of real and imaginary parts of elastic modulus of the control HL-1 cells, respectively. The median values of 336 beads at different frequency were used for the fitting. The best estimation of parameters of the control cells is $G_0 = 1.850 \times 10^4$, $\Phi_0 = 2.748 \times 10^7$, x = 1.150, and $\mu = 0.954$. At low frequency range (<1 Hz), an obvious stiffening in loss modulus was observed, which deviates from the mechanical model. Compared to the other types of cells, 17 the HL-1 cardiomyocytes exhibit a higher meta-stability of intracellular interactions or a lower agitation, seen as a smaller x (x = 1.150 compared to 1.173-1.204 reported in other cell types by Fabry et al.). Similar to the finding in Ref. 17, the values of G_0 and Φ_0 can be regarded as invariants for the same type of cell under different experimental conditions. Therefore, only the parameters x and μ were used as free fitting variables. The parameters G_0 and Φ_0 were fixed to the values obtained from the control sample. In order to evaluate the quality of fitting, the parameter r² (coefficient of determination) was calculated, of which value closer to 1 indicates better fitting. The r² for the control and blebbistatin treated cells were 0.973 and 0.967, respectively. The summations of squared errors (in log scale) between experimental measurement and the SGR model's prediction at all frequencies were 0.346 and 0.540 for the control and blebbistatin treated cells, respectively. As shown in Fig. 5, after the treatment with blebbistatin, the cells were softened by ~20% at low frequency. Moreover, after the inhibition of myosin, the stiffening at low frequency disappeared. This indicates that the stiffening mainly depends on the prestress generated by myosin activity. Besides, the cells become more fluid-like, both the viscosity (from 0.954 to 1.137) and parameter x (from 1.150 to 1.161) increased. Unlike blebbistatin, the stiffness of cells increased after fixation by paraformaldehyde. Although the twisting field B_t was set to 60 G, only 74 beads out of 185 chosen beads fell in our measurement range, whereas the ratio of usable beads to total beads on control cells was 336/420. The main reason for disqualification was failure to meet the minimum displacement threshold of 10 nm. The cell elastic shear modulus shows a smaller dependence on the frequency, which is assumed to be a more solid-like

FIG. 4. (a) Dependency of displacement amplitude and phase lag on the twisting field B_t . (b) Bead responses in the parallel and perpendicular direction of the cell protrusion. The data are from the bead in the orange box in the inset image. The scale in the inset image is 20 μ m. (c) Displacement distribution of the beads. The histogram is fit by a Gauss function (dotted line). (d) Phase lag distribution of the beads. The histogram is fit by a Gauss function (dotted line).

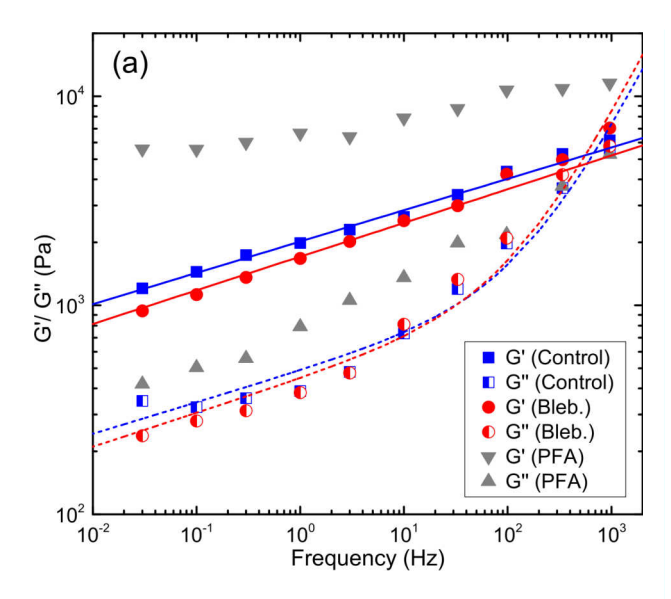


FIG. 5. The elastic shear moduli and loss moduli of control HL-1 cells (N = 336 beads), blebbistatin (50 μ M) treated cells (N = 188), and paraformaldehyde (4%) treated cells (N = 74). The blue and red lines (dot) represent the fitting results according to SGR model for control and blebbistatin treated cells, respectively. The unpaired t-tests between the control and the blebbistatin treated cells show significant differences (with p <0.037 at all frequencies \leq 10 Hz).

IV. SUMMARY AND OUTLOOK

In conclusion, we extended our previously reported magnetic tweezers setup based on a hexapole electromagnet to include 2D optical MTC functionality for twisting ferromagnetic beads. In our MTC, when the twisting field is less than 100 G, good linearity and small phase error can be achieved for frequencies up to 1 kHz. Even at high magnetic fields, coil heating was found to have no effect on cell viability. With this setup, the mechanical properties of HL-1 cardiomyocytes were characterized. In agreement with the previous findings with magnetic tweezers, this type of cell shows a log-normal distribution of stiffness and high anisotropy. Furthermore, their complex elastic moduli follow the soft glassy rheology model.

In this work, we adopted an electromagnet with magnetic field feedback control to polarize the beads. With this method, it is easy to achieve a high remanent magnetic moment with a high polarization field. In practice, it is not convenient for a single sample to do a long time measurement. Because of the magnetic relaxation, the sample needs to be transferred to the polarization apparatus for re-magnetization. However, in principle, it is possible to embed a small magnetizing coil underneath the fluidic reservoir and perform on-site magnetization using a surge generator.

ACKNOWLEDGMENTS

This work was performed in part at the Helmholtz Nanoelectronic Facility of Forschungszentrum Juelich. La Chen acknowledges support by the China Scholarship Council (No. 201206890062).

- ¹B. Fabry, G. N. Maksym, S. A. Shore, P. E. Moore, R. A. Panettieri, J. P. Butler *et al.*, "Time course and heterogeneity of contractile responses in cultured human airway smooth muscle cells," J. Appl. Physiol. **91**, 986–994 (2001), see http://jap.physiology.org/content/91/2/986.long.
- ²N. Desprat, A. Richert, J. Simeon, and A. Asnacios, "Creep function of a single living cell," Biophys. J. **88**, 2224–2233 (2005).
- ³P. Čai, Y. Mizutani, M. Tsuchiya, J. M. Maloney, B. Fabry, K. J. Van Vliet *et al.*, "Quantifying cell-to-cell variation in power-law rheology," Biophys. J. **105**, 1093–1102 (2013).
- ⁴L. Chen, V. Maybeck, A. Offenhausser, and H. J. Krause, "Characterization of the mechanical properties of HL-1 cardiomyocytes with high throughput magnetic tweezers," Appl. Phys. Lett. **107**, 053703 (2015).
- ⁵O. Medalia, I. Weber, A. S. Frangakis, D. Nicastro, G. Gerisch, and W. Baumeister, "Macromolecular architecture in eukaryotic cells visualized by cryoelectron tomography," Science **298**, 1209–1213 (2002).
- ⁶B. Fabry, G. N. Maksym, J. P. Butler, M. Glogauer, D. Navajas, and J. J. Fredberg, "Scaling the microrheology of living cells," Phys. Rev. Lett. **87**, 148102 (2001).
- ⁷J. M. Maloney and K. J. Van Vliet, "On the origin and extent of mechanical variation among cells," arXiv: 1104.0702v2 (2011).
- ⁸M. Puig-de-Morales, E. Millet, B. Fabry, D. Navajas, N. Wang, J. P. Butler *et al.*, "Cytoskeletal mechanics in adherent human airway smooth muscle cells: Probe specificity and scaling of protein-protein dynamics," Am. J. Physiol.: Cell Physiol. **287**, C643–C654 (2004).
- ⁹B. D. Hoffman and J. C. Crocker, "Cell Mechanics: Dissecting the physical responses of cells to force," Annu. Rev. Biomed. Eng. 11, 259–288 (2009).
- ¹⁰K. C. Neuman and A. Nagy, "Single-molecule force spectroscopy: Optical tweezers, magnetic tweezers and atomic force microscopy," Nat. Methods 5, 491–505 (2008).
- ¹¹J. C. Crocker and B. D. Hoffman, "Multiple-particle tracking and two-point microrheology in cells," Methods Cell Biol. 83, 141–178 (2007).

- ¹²L. Chen, A. Offenhausser, and H. J. Krause, "An inspection of force reduction in high force electromagnetic tweezers made of FeCo-V foil by laser cutting," J. Appl. Phys. 118, 124701 (2015).
- ¹³L. Chen, A. Offenhausser, and H. J. Krause, "Magnetic tweezers with high permeability electromagnets for fast actuation of magnetic beads," Rev. Sci. Instrum. 86, 044701 (2015).
- ¹⁴P. A. Valberg and J. P. Butler, "Magnetic particle motions within living cells—Physical theory and techniques," Biophys. J. 52, 537–550 (1987).
- ¹⁵P. A. Valberg and H. A. Feldman, "Magnetic particle motions within living cells—Measurement of cytoplasmic viscosity and motile activity," Biophys. J. 52, 551–561 (1987).
- ¹⁶N. Wang, J. P. Butler, and D. E. Ingber, "Mechanotransduction across the cell-surface and through the cytoskeleton," Science 260, 1124–1127 (1993).
- ¹⁷B. Fabry, G. N. Maksym, J. P. Butler, M. Glogauer, D. Navajas, N. A. Taback *et al.*, "Time scale and other invariants of integrative mechanical behavior in living cells," Phys. Rev. E 68, 041914 (2003).
- ¹⁸S. H. Hu, L. Eberhard, J. X. Chen, J. C. Love, J. P. Butler, J. J. Fredberg *et al.*, "Mechanical anisotropy of adherent cells probed by a three-dimensional magnetic twisting device," Am. J. Physiol.: Cell Physiol. 287, C1184–C1191 (2004).
- ¹⁹Y. Chung and J. Galayda, "Effect of eddy current in the laminations on the magnet field," LS Note No. 200, Argonne National Laboratory, 1992, see https://www1.aps.anl.gov/icms_files/lsnotes/files/APS_1417924.pdf.
- ²⁰B. Fabry, G. N. Maksym, R. D. Hubmayr, J. P. Butler, and J. J. Fredberg, "Implications of heterogeneous bead behavior on cell mechanical properties measured with magnetic twisting cytometry," J. Magn. Magn. Mater. 194, 120–125 (1999).
- ²¹V. L. De los Santos, J. Llandro, D. Lee, T. Mitrelias, J. J. Palfreyman, T. J. Hayward *et al.*, "Magnetic measurements of suspended functionalised ferromagnetic beads under DC applied fields," J. Magn. Magn. Mater. **321**, 2129–2134 (2009).
- ²²S. M. Mijailovich, M. Kojic, M. Zivkovic, B. Fabry, and J. J. Fredberg, "A finite element model of cell deformation during magnetic bead twisting," J. Appl. Physiol. 93, 1429–1436 (2002).